Mitochondrial Matrix Phosphoproteome: Effect of Extra Mitochondrial Calcium†

Rachel K. Hopper,‡ Stefanie Carroll,‡ Angel M. Aponte,§ D. Thor Johnson,|| Stephanie French,‡ Rong-Fong Shen,§ Frank A. Witzmann,|| Robert A. Harris,|| and Robert S. Balaban*,‡

Laboratory of Cardiac Energetics and Proteomics Core Facility, National Heart, Lung and Blood Institute, National Institutes of Health, Department of Health and Human Services, Bethesda, Maryland 20892, and Department of Biochemistry and Molecular Biology, Indiana University School of Medicine, Indianapolis, Indiana 46202-2111

Received December 3, 2005

ABSTRACT: Post-translational modification of mitochondrial proteins by phosphorylation or dephosphorylation plays an essential role in numerous cell signaling pathways involved in regulating energy metabolism and in mitochondrion-induced apoptosis. Here we present a phosphoproteomic screen of the mitochondrial matrix proteins and begin to establish the protein phosphorylations acutely associated with calcium ions (Ca^{2+}) signaling in porcine heart mitochondria. Forty-five phosphorylated proteins were detected by gel electrophoresis−mass spectrometry of Pro-Q Diamond staining, while many more Pro-Q Diamond-stained proteins evaded mass spectrometry detection. Time-dependent ^{32}P incorporation in intact mitochondria confirmed the extensive matrix protein phosphoryation and revealed the dynamic nature of this process. Classes of proteins that were detected included all of the mitochondrial respiratory chain complexes, as well as enzymes involved in intermediary metabolism, such as pyruvate dehydrogenase (PDH), citrate synthase, and acyl-CoA dehydrogenases. These data demonstrate that the phosphoproteome of the mitochondrial matrix is extensive and dynamic. Ca^{2+} has previously been shown to activate various dehydrogenases, promote the generation of reactive oxygen species (ROS), and initiate apoptosis via cytochrome *c* release. To evaluate the Ca^{2+} signaling network, the effects of a Ca^{2+} challenge sufficient to release cytochrome *c* were evaluated on the mitochondrial phosphoproteome. Novel Ca^{2+}-induced dephosphorylation was observed in manganese superoxide dismutase (MnSOD) as well as the previously characterized PDH. A Ca^{2+} dose-dependent dephosphorylation of MnSOD was associated with an ∼2-fold maximum increase in activity; neither the dephosphorylation nor activity changes were induced by ROS production in the absence of Ca^{2+}. These data demonstrate the use of a phosphoproteome screen in determining mitochondrial signaling pathways and reveal new pathways for Ca^{2+} modification of mitochondrial function at the level of MnSOD.

Mitochondria are thought to be the result of an early interaction of two lines of cellular life, the bacterium and eukaryotic cell (*1*, *2*). At this point in time, mitochondria play a critical role in energy metabolism, apoptosis, and cell signaling pathways in the cell. However, the acute and chronic regulatory mechanisms of this organelle remain poorly defined. One approach to assessing the function and regulation of the mitochondrion is an evaluation of the mitochondrial proteome. Estimates predict up to 3000 proteins (*3*, *4*) in mitochondria; however, recent large-scale screening studies by Taylor (*5*) and Mootha (*6*) identified only ∼600 distinct mitochondrial proteins. Many have used proteomic approaches to evaluate differential protein expression in mitochondria to provide insight into chronic responses to perturbations and disease (for examples, see refs *7* and *8*). The rapid response by mitochondria to changes in energy demand and other environmental factors suggests that acute regulatory pathways are also important in mitochondrial function. Phosphorylation events regulated by networks of kinases and phosphatases are currently believed to be among the most prevalent acute regulatory modifications within the cell (*9*−*11*). Many mitochondrial proteins have been demonstrated or proposed to be regulated by protein phosphorylation, including pyruvate dehydrogenase (PDH) (*12*) and components of the respiratory chain complexes (*13*−*18*). A phosphoproteome screen of potato mitochondrial membranes using radiolabeled ATP found a wide range of dynamically phosphorylated proteins, suggesting that the phosphorylation mechanism is extensively used in the mitochondrial matrix (*19*). Information about the distribution of kinases and phosphatases within mitochondria is limited. Until recently, mitochondrial enzymes PDH kinase and branched-chain α-ketoacid dehydrogenase kinase were thought to be the main kinases functioning in mitochondria (*20*). Recent studies indicate that several cytosolic kinases translocate into mitochondria, including protein kinase A, protein kinase C δ and ϵ isoforms, stress-activated protein kinase, and A-Raf

† Intramural Funding of the Division of Intramural Research, NHLBI, NIH, DHHS, and NIH Grant DK47844 to R.A.H.

* To whom correspondence should be addressed: Laboratory of Cardiac Energetics, National Heart, Lung and Blood Institute, National Institutes of Health, 10 Center Dr., Room B1D416, Bethesda, MD 20892-1061. Telephone: (301) 496-3658. Fax: (301) 402-2389. E-mail: rsb@nih.gov.

‡ Laboratory of Cardiac Energetics, National Heart Lung and Blood Institute, National Institutes of Health.

§ Proteomics Core Facility, National Heart Lung and Blood Institute, National Institutes of Health.

|| Indiana University School of Medicine.

10.1021/bi052475e CCC: $33.50
Published on Web 02/04/2006

kinase (*21*, *22*). Several of these kinases are activated by calcium (Ca^{2+}), a signaling molecule involved in the activation of dehydrogenases (*23*), generation of reactive oxygen species (ROS) (*24*), and initiation of apoptosis (*25*, *26*).

The purpose of this study was to characterize the phosphoproteome of porcine heart mitochondria, as detected by the Pro-Q Diamond stain using two-dimensional (2D) gel electrophoresis and ^{32}P radioisotopic analysis, as well as to perform an initial screen for mitochondrial kinases and phosphatases associated with these protein phosphorylations. Following the establishment of steady-state conditions, the effects of acute alterations in the extramitochondrial Ca^{2+} level sufficient to initiate mitochondrion-induced apoptosis were evaluated on the mitochondrial phosphoproteome to provide insight into the signaling pathways associated with the complex action of Ca^{2+} on mitochondrial function.

EXPERIMENTAL PROCEDURES

Mitochondrial Isolation. Mitochondria were isolated from pig hearts, cold-perfused in situ to remove blood and extracellular Ca^{2+} (*27*). Briefly, the hearts were harvested from anesthetized and heparinized (10 000 units iv) animals. The heart was perfused via the aorta in a retrograde fashion in situ with ~400 mL of ice-cold isolation buffer [0.28 M sucrose, 10 mM *N*-(2-hydroxyethyl)piperazine-*N*′-2-ethanesulfonic acid (HEPES), and 0.2 mM EDTA (pH 7.21)] to remove blood and reduce the level of free calcium for mitochondrial isolation. The perfused heart was weighed, and the left ventricle was dissected free of fat, large vessels, and the right ventricular free wall. Sections of the left ventricle (4−5 g) were minced in 20 mL of isolation buffer. Trypsin (2.5 mg) was then added, and the tissue was incubated for 15 min at 4 °C. The digestion was stopped by adding 20 mL of isolation buffer with 1 mg/mL bovine serum albumin (BSA) and 13 mg of trypsin inhibitor. The suspension was decanted, and the remaining tissue was resuspended in 20 mL of ice-cold isolation buffer with 1 mg/mL BSA. The tissue was homogenized with a loose-fitting Teflon homogenizer (two times) followed by a tight-fitting Teflon pestle (five times). The homogenate was centrifuged at 600*g* for 10 min at 4 °C, and the supernatant was decanted and centrifuged at 8000*g* for 15 min. The buffy coat was removed, and the pellet was resuspended in 20 mL of ice-cold isolation buffer with 1 mg/mL BSA. The wash-and-centrifugation step was repeated twice, once in the presence of 1 mg/mL BSA and the final time in the absence of BSA. The final pellet was resuspended in 137 mM KCl, 10 mM HEPES, and 2.5 mM $MgCl_2$ (pH 7.2) (experimental buffer) and stored on ice. It should be noted that this preparation created with a trypsin digestion represents a mixed population of mitochondria from the heart (*28*). Experiments on mitochondria isolated with the same procedure without trypsin resulted in a much lower yield and very different protein profiles (not shown), suggesting that different pools of mitochondrial proteomes are present in the heart consistent with previous studies (*29*, *30*). No evidence of protein fractionation by trypsin was evident in comparing the tyrpsin and non-trypsin preparations, suggesting that the trypsin treatment was not significantly influencing these results. All procedures that were performed were in accordance with the guidelines described in the Animal Care and Welfare Act (7 USC 2142 § 13).

Mitochondrial Function and Cytochrome c Release. The rate of mitochondrial oxygen consumption was determined at 37 °C using a closed water-jacketed reaction chamber containing a Clark oxygen electrode as previously described (*27*). Most experiments were conducted in an oxygen-saturated buffer containing 125 mM KCl, 15 mM NaCl, 20 mM HEPES, 1 mM EGTA, 1 mM EDTA, and 5 mM $MgCl_2$ (pH 7.1) (buffer A). Mitochondria were allowed to equilibrate in the reaction chamber with buffer A for 6 min to permit Ca^{2+} depletion before addition of carbon substrates [glutamate (5 mM) and malate (5 mM)] (*27*).

Ca^{2+}-dependent cytochrome *c* (cyt *c*) release was used as a marker of mitochondrial induction of apoptosis. Cyt *c* release was assessed spectrophotometrically by quantifying the removal of cyt *c* from mitochondrial pellets. After each experimental perturbation, mitochondria were pelleted at 15800*g* and stored at −80 °C for later analysis. Mitochondrial pellets were resuspended [1 nmol of cytochrome *a* (cyt *a*)/mL] in buffer A containing 5 μM antimycin A, 5 mM glutamate/malate, and 1% Triton X-100. Antimycin A was added to prevent electron flow to cyt *c*, resulting in highly oxidized states. Glutamate/malate was used to maximally reduce cytochrome *b* and FAD. Triton X-100 was used to minimize light scattering (*31*). The mitochondrial cyt *c* (550 nm) and cyt *a* (605 nm) content was determined from difference absorption spectra of the suspension in the presence and absence of sodium hydrosulfite to maximally reduce cyt *c* and cyt *a*, respectively. The mitochondrial cyt *c* content is reported as the relative 550 nm peak area versus the 605 nm peak area of cyt *a*. It is important to note that since cytochrome *b* was held fully reduced under both conditions it did not interfere with this determination.

The dependence of Ca^{2+}-induced cyt *c* release on ATP, ADP, and P_i is highly variable in the literature. Thus, we determined these interdependencies for this preparation. Combinational dose−response curves for cyt *c* release 5 min after addition of Ca^{2+} were determined using P_i, ADP, ATP, and Ca^{2+}. These studies revealed that ADP had little or no effect on this process, while 5 mM P_i and 10 mM ATP were found to generate an optimal release of cyt *c* in the presence of 100 μM free Ca^{2+} (see the Results). Free Ca^{2+} levels were determined using the MaxChelator software for the elements in buffer A. In separate experiments, the time course of cyt *c* release was evaluated under these optimal conditions (buffer A with 5 mM P_i, 10 mM ATP, and 100 μM Ca^{2+}) and found to plateau approximately 5 min after Ca^{2+} addition. Thus, the conditions used for evaluating Ca^{2+}-induced cyt *c* release were 100 μM free Ca^{2+}, 5 mM P_i, and 10 mM ATP added after the 6 min depletion conditions outlined above. The controls were identical with the omission of Ca^{2+}. Inhibition of Complex I was achieved by adding 6 μM rotenone and 3 mM succinate in lieu of Ca^{2+} and incubating the mixture for 5 min.

^{32}P Labeling Experiments. To investigate the dynamics of ^{32}P labeling of mitochondrial matrix proteins, experiments were performed to expose matrix proteins to physiological levels of ATP labeled in the γ position with ^{32}P ($^{32}P\gamma$ATP). The experimental rationale was to add ^{32}P as inorganic phosphate (P_i) to fully energized mitochondria. The P_i is transported into the matrix and used to synthesize $^{32}P\gamma$ATP by oxidative phosphorylation. It was assumed that this would provide a very high specific activity of the millimolar matrix

ATP. This was accomplished by adding 0.75 mCi of $^{32}P_i$ to 15 mg of mitochondrial protein in 3 mL of buffer A in the absence of ATP or cold P_i in the presence of 5 mM G/M. The mitochondria were allowed to incubate for 5−20 min, at which time an aliquot was removed and the reaction was quenched with 5% TCA at 0 °C with 5 mM KF. In some samples, 0.1 mM dinitrophenol was added after the 20 min labeling period with $^{32}P_i$ and the incubation extended for additional 5 min to uncouple mitochondria, and the reaction was then quenched as described above. Samples were pelleted at 10000*g*. Mitochondrial pellets (3 mg of protein) were solubilized with 100 μL of 1% SDS (w/v) in 100 mM Tris-HCl (pH 7.0) at 95 °C. Pellets were incubated at 95 °C for 5 min followed by cooling on ice for 5 min. A chloroform/methanol precipitation was performed to remove salts, lipids, and free $^{32}P_i$ or $^{32}P\gamma$ATP (*32*) by adding 6 mL of methanol, 150 μL of chloroform, and 450 μL of dH_2O to each pellet, vortexing between each addition. Samples were centrifuged for 5 min at 12000*g*, and the supernatant was discarded. Precipitated protein was washed again by centrifugation in 450 μL of methanol.

2D Gel Electrophoresis and Gel Staining. Samples were run differently for the radioisotopic and Pro-Q Diamond and Sypro Ruby straining procedures. For Pro-Q staining, mitochondrial pellets (1 nmol of cyt *a*) were solubilized with 100 μL of 1% SDS (w/v) in 100 mM Tris-HCl (pH 7.0) at 95 °C. Pellets were sonicated five times for 3 s each or until they were dissolved. Pellets were incubated at 95 °C for 5 min followed by cooling on ice for 5 min. A chloroform/methanol precipitation was performed to remove salts and lipids (*32*) by adding 600 μL of methanol, 150 μL of chloroform, and 450 μL of dH_2O to each pellet, vortexing between each addition. Samples were centrifuged for 5 min, and the supernatant was discarded. Precipitated protein was washed again by centrifugation in 450 μL of methanol. The supernatant was discarded, and pellets were resuspended in 100 μL of buffer containing 30 mM Tris-HCl, 7 M urea, 2 M thiourea, and 4% CHAPS (w/v). Samples were pooled at this stage to obtain adequate protein (500 μg/gel) for paired 2D gel analysis. Because protein is lost during this precipitation procedure, the correlation between cyt *a* content and total protein may no longer be valid. Therefore, the total amount of protein in each sample was determined using the Amersham Quant kit (Amersham Biosciences, Piscataway, NJ). For each sample, 500 μg of total protein in 440 μL of rehydration solution [7 M urea, 2 M thiourea, 4% CHAPS (w/v), 1% De-streak reagent (v/v), and 2% (pH 3−10 NL) Pharmalyte (v/v)] was loaded onto 24 cm Immobiline DryStrip gels (pH 3−10 NL). Isoelectric focusing was achieved by active rehydration for 12 h at 30 V followed by stepwise application of 500, 1000, and 8000 V for a total of ∼70000 Vh (Ettan IPG Phor, Amersham). Immobiline DryStrip gels were equilibrated in 10 mL of SDS equilibration solution [50 mM Tris-HCl (pH 8.8), 6 M urea, 30% glycerol, and 2% SDS] for 10 min, first containing 0.5% DTT and then with 4.5% iodoacetemide. Gel strips were applied to 12.5% SDS−PAGE gels and sealed with 0.5% agarose containing bromophenol blue. Electrophoresis was performed in an Ettan DALT-12 tank (Amersham) in electrophoresis buffer consisting of 25 mM Tris (pH 8.3), 192 mM glycine, and 0.2% SDS until the dye front advanced completely (∼1750 Vh). Gels were fixed overnight in 500 mL in a solution of 10% TCA and 30% methanol. The fix solution was changed once. Following four 15 min washes in 1 L of warm water each, gels were stained with 500 mL of Pro-Q Diamond (Molecular Probes, Eugene, OR) for 3 h and destained using four 1 h washes with 500 mL of destain containing 50 mM sodium acetate and 10% acetonitrile. Following image acquisition, gels were stained with Sypro Ruby protein gel stain (Bio-Rad Laboratories, Hercules, CA).

For the radioisotope studies, mitochondrial protein was suspended to a concentration of 500 μg in 500 μL of a solution containing rehydration buffer [8 M urea, 2% CHAPS, 15 mM DTT, 0.2% ampholytes (pH 3−10), and 0.001% orange G]. The 500 μL protein dilutions were loaded onto IPG strips (24 cm, linear pH 3−10) by overnight, passive rehydration at room temperature. Isoelectric focusing was performed simultaneously on all IPG strips using the Protean IEF Cell (Bio-Rad), by a program of progressively increasing voltage (150 V for 2 h, 300 V for 4 h, 1500 V for 1 h, 5000 V for 5 h, 7000 V for 6 h, and 10 000 V for 3 h) for a total of 100 000 Vh. A computer-controlled gradient casting system was used to prepare 2D SDS gradient slab gels (20 cm × 25 cm × 0.15 cm) in which the acrylamide concentration varied linearly from 8 to 15% T. One-dimensional (1D) IPG strips were loaded directly onto the slab gels following equilibration for 10 min in equilibration buffer I [6 M urea, 2% SDS, 0.375 M Tris-HCl (pH 8.8), 20% glycerol, and 130 mM DTT] and 10 min in equilibration buffer II [6 M urea, 2% SDS, 0.375 M Tris-HCl (pH 8.8), 20% glycerol, and 135 mM iodoacetamide]. 2D slab gels were run in parallel at 4 °C for 18 h at 160 V. Slab gels were stained using a colloidal Coomassie Blue G-250 procedure. Gels were fixed in 1.5 L of a 50% ethanol/2% phosphoric acid mixture overnight followed by three 30 min washes in 2 L of deionized water. Gels were transferred to 1.5 L of a 30% methanol/17% ammonium sulfate/3% phosphoric acid mixture for 1 h followed by addition of 1 g of powdered Coomassie Blue G-250 stain (*33*). After 96 h, gels were washed several times with water. Gels were allowed to equilibrate overnight in a 5% glycerol solution and then dried in a large format gel dryer for 6 h at 65 °C under a vacuum. Dried gels were placed in a film development cassette (Kodak) for 5 days with three sheets of 8 × 10 maximum-sensitivity film (Kodak).

Image Acquisition and Analysis. For Pro-Q Diamond and Supro Ruby analysis, gels were scanned on a Typhoon 9400 variable mode imager (Amersham) at a resolution of 100 μm. Excitation was at 532 nm with emission filters of 610BP30 for Sypro Ruby and 580BP30 for Pro-Q Diamond. Image analysis was performed using single-stain analysis with intelligent noise correction algorithm (INCA) processing by Progenesis Discovery software (Nonlinear Dynamics, Newcastle upon Tyne, U.K.). Radiograms and dried gels were scanned on an Epson CX5400 high-resolution scanner.

The Ettan Spot Handling Workstation performed automated extraction and in gel trypsin digestion of selected protein spots according to Amersham instructions. Peptides were analyzed using a mass spectrometer (4700 Proteomics Discovery System, Applied Biosystems, Foster City, CA) using MALDI-TOF and MS/MS. At least two peptides were obtained for each protein using MS/MS. Proteins were identified from the acquired spectra using the MASCOT database search function.

Enzyme Activity Assays. The activity of manganese superoxide dismutase (MnSOD) was measured spectroscopically using a commercially available assay kit (Trevigen, Gaithersburg, MD). Superoxide anions generated by the conversion of xanthine to uric acid and hydrogen peroxide by xanthine oxidase in turn convert NBT to NBT-diformazan, which absorbs light at 550 nm. MnSOD activity was measured in both control and high-Ca^{2+}-treated mitochondrial pellets by the reduction of NBT-diformazan, as indicated by a decrease in A_{550}.

PDH activity was determined by following NADH production in the presence of pyruvate, coenzyme A, and NAD (*34*). Mitochondrial pellets from control and high-Ca^{2+} experiments were resuspended in a small volume and pulverized to disrupt membranes. Mitochondrial matrix elements were exposed by freezing the mitochondrial suspension in liquid nitrogen and pulverizing the frozen pellet using a tissue Bessman pulverizer (BioSpec Products Inc., Bartlesville, OK). The thawing and freeze-pulverizing cycle was repeated two times. PDH activity was assayed in a reaction mixture (pH 8.0) containing 50 mM Tris, 10 mM pyruvate, 0.2 mM coenzyme A, 2 mM NAD, 2 mM cocarboxylase, 1 mM $MgCl_2$, and pulverized mitochondria at a concentration of 0.2−0.4 nmol of cyt *a*/mL. The reaction was carried out at 37 °C and was initiated with coenzyme A. Production of NADH was assessed spectrophotometrically by monitoring A_{350}.

H_2O_2 Production. The level of H_2O_2 was measured fluorometrically using the Amplex Red Hydrogen Peroxide Assay Kit (Molecular Probes). The production of H_2O_2, as indicated by the conversion of Amplex Red to resorufin, was monitored under control and high-Ca^{2+} conditions for 10 min. The fluorescence intensity was measured with a fluorometer (FL3-22, Jobin-Yvon Horiba, Edison, NJ) using excitation and emission wavelengths of 545 and 590 nm, respectively.

Screen for Kinases and Phosphatases. Mitochondrial pellets were suspended in lysis buffer (20 mM Tris, 40 mM glycerophosphate, 30 mM sodium fluoride, 20 mM sodium pyrophosphate, 5 mM EDTA, 2 mM EGTA, 1 mM sodium orthovanadate, 0.5% Triton X-100, and 1 mM DTT) supplemented with 1 mM phenylmethanesulfonyl fluoride, 2 mg/mL leupeptin, 4 mg/mL aprotinin, and 1 mg/mL pepstatin A and sonicated for 15 s. Debris was removed by centrifugation at 100 000 rpm for 30 min at 4 °C. The protein concentration of the resulting supernatant was determined using the Amersham Quant kit. Kinetworks analyses (Kinexus Bioinformatics Corp., Vancouver, BC) were performed on 300−600 μg of protein/sample by SDS−PAGE and subsequent immunoblotting with panels of up to three primary antibodies per channel in a 20-lane multiblotter. The Kinetworks analyses screened for 75 kinases (KPKS 1.2) and 25 phosphatases (KPPS 1.2).

RESULTS

Initial studies were conducted to determine what proteins of the mitochondrial proteome are resolved and detected using our 2D gel electrophoresis system. From gels stained for total protein with Sypro Ruby, we identified mitochondrial proteins of various functions, including intermediary metabolism, β-oxidation, amino acid biosynthesis, complexes of oxidative phosphorylation, transport proteins, including chaperones, etc., consistent with what has previously been reported in mouse brain, heart, kidney, and liver (*6*) and human heart (*5*) mitochondria. Because the pig genome has not been fully sequenced, we were unable to identify some proteins on the basis of existing porcine sequence data and therefore used other mammalian database information because many mitochondrial proteins are highly conserved across species. Some proteins were unable to be identified using these methods, despite a relative protein abundance, suggesting extensive gene splicing or post-translational modifications complicating the identifications. Similar problems have been noted in prior studies (*6*, *7*).

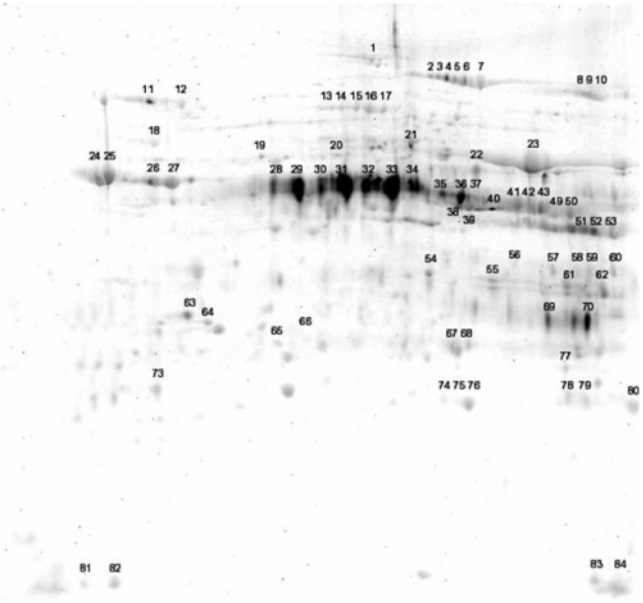

FIGURE 1: Two-dimensional gel electrophoresis and staining of the phosphoproteome of porcine heart mitochondria with Pro-Q Diamond phosphoprotein gel stain. Proteins are separated by isoelectric point (pI), from pH ~4 to 9 along the horizontal axis, and by molecular mass, from ~100 to 10 kDa, vertically. Numbers refer to the protein identifications presented in Table 1. Not all Pro-Q Diamond-stained proteins were identified due to a failure to reach statistical significance in the mass spectrometry analysis.

Two strategies were used for detecting phosphorylated proteins. Pro-Q Diamond was used to stain for phosphorylated proteins independent of protein turnover. ^{32}P labeling was used to examine the dynamics of matrix protein phosphorylation and provide confirmation of protein phosphorylations found in the more indirect Pro-Q Diamond staining approach for those proteins with adequate phosphate turnover. The sensitivity of Pro-Q Diamond for serine, threonine, and tyrosine phosphorylation has been validated in several systems (*35*, *36*). Most recently, it has been used to characterize the global effects on protein phosphorylation in response to alterations of cellular kinases (*37*). A representative gel of mitochondrial proteins stained with Pro-Q Diamond is shown in Figure 1. Automatic spot detection showed ~200 phosphorylated spots per gel with Pro-Q Diamond staining. However, the total number of proteins was fewer than 200 since many proteins had a distribution of spots generated by the isoelectric focusing caused by multiple phosphorylations, as observed with aconitase or pyruvate dehydrogenase, or other phenomena such as differential oxidation. We considered a positive identification to be indicated by >95% confidence in the MASCOT identification. Using these criteria, 45 separate

Table 1: Porcine Heart Mitochondrial Proteins Stained with Pro-Q Diamond

functional category	spot number	protein name	NCBI accession number	molecular mass (kDa)	pI
		Oxidative Phosphorylation			
Complex I	11, 12	NADH dehydrogenase (ubiquinone) Fe−S protein 1 (75 kDa)	51858651	80 331	5.7
	22	NADH dehydrogenase (ubiquinone) flavoprotein 1	23574759	51 322	8.5
	60	NADH dehydrogenase (ubiquinone) 1α subcomplex, 9 (39 kDa)	13097156	38 475	9.7
	65	NADH dehydrogenase 24 kDa subunit	1364245	23 771	5.7
	73	NADH-ubiquinone oxidoreductase 23 kDa subunit, mitochondrial precursor	2499325	24 203	6.0
	78	NADH dehydrogenase (ubiquinone) 1*β* subcomplex, 10 (22 kDa)	28461255	21 237	8.7
	84	NADH-ubiquinone oxidoreductase 15 kDa subunit (Complex I − 15 kDa)	400587	12 888	9.0
Complex II	13−17	succinate dehydrogenase [ubiquinone] flavoprotein subunit, mitochondrial precursor	1352262	74 371	7.3
	72	succinate dehydrogenase Ip subunit	27716317	32 607	9.0
Complex III	26, 27	ubiquinol−cytochrome *c* reductase complex core protein I, mitochondrial precursor	10720406	53 444	5.9
	40, 43	ubiquinol-cytochrome *c* reductase core protein II	27807143	48 233	8.8
	67	ubiquinol-cytochrome *c* reductase, Rieske iron−sulfur protein precursor	111883	27 956	8.9
	83	ubiquinol-cytochrome *c* reductase binding protein	34866011	13 550	9.3
Complex IV	81, 82	cytochrome *c* oxidase polypeptide Va	117097	12 485	5.0
F_0F_1-ATPase	23	ATP synthase, mitochondrial F_1 complex, α subunit	15030240	59 886	9.1
	24, 35	ATP synthase, mitochondrial F_1 complex, *β* subunit precursor	32189394	56 525	5.3
	62	ATP synthase *γ* subunit precursor	162717	32 993	9.4
	19, 20	chain C, bovine mitochondrial F_0F_1-ATPase	33357743	55 313	8.3
	79, 80	H^+-ATPase subunit, oligomysin sensitivity-conferring protein	913531	20 932	9.8
		Intermediary Metabolism			
Krebs cycle	51−53	aspartate aminotransferase, mitochondrial precursor	112985	47 805	9.1
	2−7	aconitate hydratase, mitochondrial precursor	113159	86 449	8.2
	39	citrate synthase, chain B	230994	49 116	7.0
	42, 49, 50	isocitrate dehydrogenase (NADP-dependent)	284570	47 895	8.7
	56−59	malate dehydrogenase	65932	33 518	8.6
	1	2-oxoglutarate dehydrogenase	2160381	114 602	6.6
	69, 70	dihydrolipoyllysine-residue succinyltransferase component of 2-oxoglutarate dehydrogenase complex	266684	47 668	8.2
	28−34	pyruvate dehydrogenase, E1α subunit	448580	41 056	6.8
fatty acid oxidation	47	acyl-CoA dehydrogenase, long-chain-specific, mitochondrial precursor (LCAD)	2829676	48 326	7.0
	21	dihydrolipoyldehydrogenase, mitochondrial precursor	1706444	54 689	8.0
	71	electron transfer flavoprotein, *β* subunit precursor	35384838	27 974	8.6
	68	enoyl-CoA hydratase, short chain	49257190	31 952	8.9
	8−10	gastrin-binding protein	47522754	83 738	9.3
	61	chain C, pig heart short-chain L-3-hydroxyacyl-CoA dehydrogenase	6435806	32 823	8.7
	77	hydroxyacyl-CoA dehydrogenase, type II	27805907	27 294	8.5
	44, 45	long-chain 3-ketoacyl-CoA thiolase	47522760	47 727	9.3
	46	chain A, medium-chain acyl-CoA dehydrogenase (MCAD)	640350	42 629	6.5
	48	short-chain acyl-CoA dehydrogenase (SCAD)	47522686	45 221	8.4
		Transport			
	18	chaperonin; mitochondrial protein P1 precursor	90207	61 122	5.8
	55	voltage-dependent anion channel 1	47522750	30 822	8.6
	54	voltage-dependent anion channel 2	55664661	30 842	8.0
		Antioxidant			
	74−76	Mn superoxide dismutase	15082142	11 795	7.0
	66	thioredoxin-dependent peroxide reductase, mitochondrial precursor	2507170	28 406	7.2
		Other			
	37	sarcomeric mitochondrial creatine kinase precursor	4502855	48 004	8.5
	35, 36, 41	creatine kinase, mitochondrial 2	38174368	47 899	8.6
	63, 64	prohibitin	4505773	29 843	5.6

proteins were identified by mass spectrometry analysis, accounting for a majority of the observed proteins. Proteins that were identified included all of the complexes of oxidative phosphorylation, numerous enzymes of intermediary metabolism, and enzymes involved in the metabolism of reactive oxygen species (Table 1). While many of these phosphorylations have been previously described, several of these phosphorylated enzymes, to our knowledge, have not been previously reported in the literature and represent unique observations. These include several complex I subunits, enzymes involved in fatty acid metabolism, and the *γ* subunit of the F_1-ATPase (γF_1). MnSOD has been shown to be phosphorylated in potato mitochondria (*19*) using radiolabeled ATP, but we have not found evidence of this

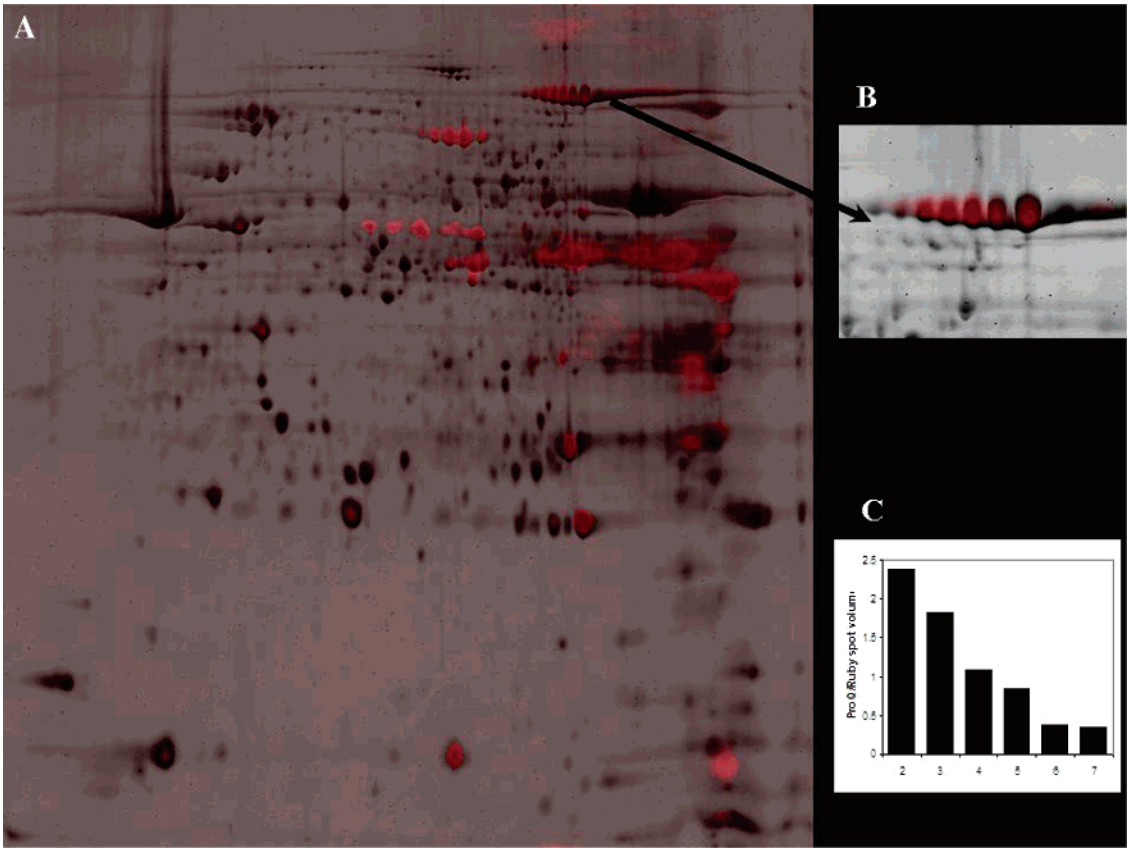

FIGURE 2: Overlay of Sypro Ruby total protein (black) and Pro-Q Diamond phosphoprotein (red) staining of the mitochondrial proteome in the absence of Ca^{2+} (A). The relative amplitude of the two channels was arbitrarily set. The majority of proteins detected with Sypro Ruby were not detected with Pro-Q Diamond, resulting in a predominance of pure black spots. Proteins heavily labeled with Pro-Q Diamond appear red with essentially no Sypro Ruby signal (for example, PDH, spots 27−33). We used the ratio of the Sypro Ruby and Pro-Q Diamond signals as a quantitative method for determining the degree of protein phosphorylation. As a control for this approach, the multiple phosphorylation states of aconitase (spots 2−7) were evaluated in panels B and C. The enhanced phosphorylation of aconitase is associated with an acid shift in its isoelectric focusing pH; taking the ratio of the Sypro Ruby stain and Pro-Q Diamond revealed a quantitative relationship between this ratio and isoelectic focus for this single protein.

phosphorylation described in mammalian systems. The Pro-Q Diamond-stained gel shows four distinct spots that were each identified as MnSOD using MS/MS, which have similar molecular masses but different isoelectric points, consistent with multiple phosphorylation states.

To relate the level of phosphorylation to protein content, Figure 2A shows an overlay of the Pro-Q (red) and Sypro Ruby (black) images, indicating the relative intensity of phosphorylation compared to the total amount of protein present for each spot. Intensely red spots are highly phosphorylated low-abundance proteins. Multiple aconitase spots (Figure 2B) reveal the relative degree of phosphorylation changing with the isoelectric focusing pH, revealed by a ratiometric approach (Figure 2C). The low abundance of some phosphorylated proteins hampered mass spectrometry identification and suggested that some proteins were better detected with Pro-Q Diamond than Sypro Ruby. A similar observation was made between Comassie stain and ^{32}P labeling below.

A representative phosphorimage of ^{32}P-labeled mitochondrial proteins and the corresponding Coomassie-stained gel are shown in panels A and B of Figure 3, respectively. Due to the wide range of ^{32}P labeling, any one exposure is not adequate to reveal all of the sites without over- or under-exposure of the film or the contrast/brightness setting in software. We have selected an intermediate exposure for this example. The proteins labeled using this approach included SOD-2, PDH E1α, citrate synthase, inhibin, MCAD, LCAD, and Rieske iron−sulfur protein (RISP) with details in the figure legend. Many of the ^{32}P-labeled proteins corresponded to observation in Pro-Q Diamond. However, there were many notable differences between ^{32}P and Pro-Q Diamond staining. Many more proteins were labeled with ^{32}P where there was no corresponding Pro-Q Diamond, Coomassie/Sypro Ruby staining, leaving a much different overall pattern in all three staining approaches. The direct comparison of the ^{32}P labeling (red) with Coomassie (green) is seen in the overlay presented in Figure 3C. At this exposure, the ^{32}P labeling was overexposed in the PDH E1α region. The region around MnSOD and RISP has been expanded in all of the panels. The correlation of the Coomassie with the ^{32}P labeling is generally poor, suggesting many low-abundance proteins with a significant number of phosphorylation sites with a high degree of turnover. These observations suggest that the overall sensitivity of the ^{32}P method is significantly higher than that of the Pro-Q Diamond method, especially for proteins with high phosphate turnover rates, while Pro-Q Diamond is more sensitive to more abundant proteins with slow turnover rates. In addition, the absolute sensitivity for Pro-Q Diamond for all phosphorylation sites should not be considered constant, as it surely is for ^{32}P labeling, since the confirmation of the relative sensitivity of Pro-Q Diamond

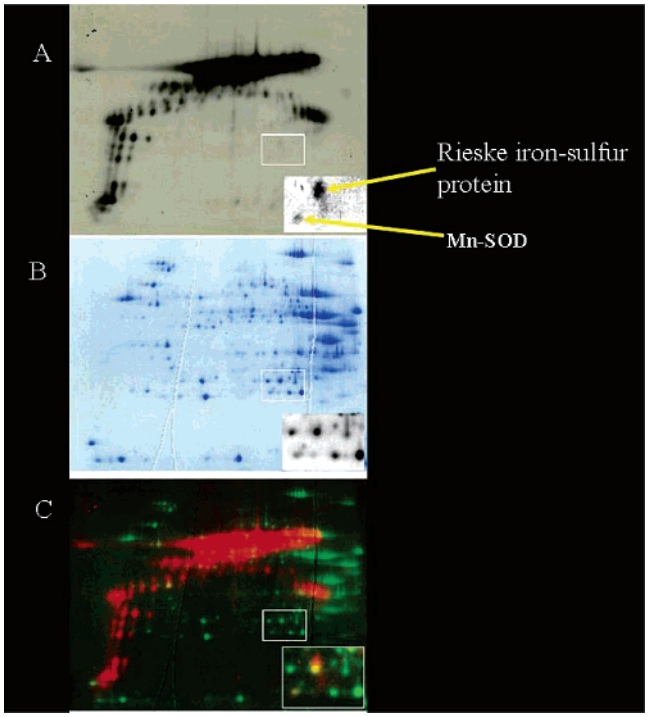

FIGURE 3: Two-dimensional gel electrophoresis and staining of the phosphoproteome of porcine heart mitochondria with [^{32}P]PO_4. Proteins are separated by isoelectric point (pI), from pH ~4 to 9 along the horizontal axis, and by molecular mass, from ~100 to 10 kDa, vertically. (A) Autoradiogram of the gel. The MnSOD−Rieske iron−sulfur region is expanded in this and all other panels at optimal contrast and brightness. (B) Coomassie stain of the same gel. (C) Color overlay of the autoradiogram (red) and Coomassie stain (green). The amplitude of both gels was arbitrarily set.

has been limited to a handful of proteins. The dependence on phosphorylation turnover can limit ^{32}P detection of phosphorylation as illustrated by the effects of incubation times of 5 and 20 min on ^{32}P labeling in Figure 4. Clearly, a longer incubation time results in more detectable phosphorylation sites. The labeling of a significant fraction of proteins in 5−20 min suggested that the turnover of the phosphorylation events was quite rapid for many proteins. To confirm the off-rate, we treated the mitochondria with uncoupler that would stimulate breakdown and inhibit synthesis of matrix ^{32}PγATP. After only 5 min, the overall level of ^{32}P labeling was significantly reduced, supporting the notion of a rapidly turning over pool of phosphorylated proteins (4C). The complete time dependence of this process is outside the scope of the current report, but this approach can clearly be applied to obtain ^{32}P turnover rates for many of these proteins. One interesting omission from the ^{32}P data was any detectable turnover of phosphorylation in aconitase or succinate dehydrogenase. Both Pro-Q Diamond and the isoelectric shift pattern of these proteins are consistent with the phosphorylation. The lack of ^{32}P labeling of these proteins suggests a very slow turnover of much more than 20 min in this preparation.

Ca^{2+} is a well-recognized second messenger in the control of mitochondrial function under both normal and pathophysiological conditions (*23*, *38*). Ca^{2+} action has often been linked to protein phosphorylation events via Ca^{2+}-sensitive kinases and phosphatases. Thus, we applied this phosphoprotein screen to evaluate the acute effects of extramitochondrial Ca^{2+} on mitochondrial protein phosphorylation. The concentration of Ca^{2+} used was selected to be sufficient to induce release of cyt *c* from mitochondria, the initial step of mitochondrion-induced apoptosis. Because it was difficult to predict the optimal extramitochondrial conditions that cause cyt *c* release with Ca^{2+} from the literature, we determined the extramitochondrial conditions of maximal Ca^{2+}-induced cyt *c* release for our system by exposing mitochondria to various concentrations of Ca^{2+} in the presence of glutamate and malate, P_i, and adenine nucleotides (ATP or ADP) while respiration and cyt *c* release were monitored. Maximal cyt *c* release occurred in the presence of 5 mM P_i, 10 mM ATP, and an excess of 100 μM free Ca^{2+}. Mitochondria released 65.7 ± 5.0% of total cyt *c* under these conditions, compared to 6.9 ± 2.7% ($P < 0.001$) release in the absence of Ca^{2+} ($n = 4$). Ca^{2+} concentrations above 100 μM did not result in a significant increase in the percent of cyt *c* released, suggesting that the amount released during this acute perturbation plateaus around 70% of the total cyt *c* content. Mitochondria released only 14.1 ± 2.2% of the total cyt *c* ($P < 0.01$, $n = 4$) in 100 μM Ca^{2+} without P_i and ATP, demonstrating that cyt *c* release depends on P_i and ATP in addition to a high concentration of free Ca^{2+}. Preincubation of mitochondria in cyclosporin A, an agent that inhibits mitochondrion-induced apoptosis by blocking the mitochondrial permeability transition pore, before exposure to high concentrations of Ca^{2+}, P_i, and ATP, resulted in release of only 36.6 ± 3.8% ($P < 0.01$, $n = 4$) of total cyt *c*, a blockage of nearly 68% of the cyt *c* release occurring under the high-Ca^{2+} conditions in the absence of this agent (data not shown). It is important to note that in these studies with 10 mM ATP in the extramitochondrial space significant ATP depletion would likely not occur even under uncoupled conditions. This is in contrast to the results of ^{32}P studies in which the total concentration of ATP was limited by the very low concentration of ^{32}P added to the sample.

The effects of Ca^{2+} on mitochondrial protein phosphorylation were determined by incubating mitochondria under the control conditions in the absence and presence of 100 μM free Ca^{2+}. The intensity of staining was given by the spot volume corrected for noise using the Progenesis Intelligent Noise Correction Algorithm (INCA), normalized for total protein content using the total spot volume of the corresponding Sypro Ruby image. Because of the signal-to-noise ratio of the Pro-Q Diamond data, we considered a significant change in phosphorylation only when the normalized area changed more than 30% in these initial studies. While most of the proteins did not exhibit a significant change in phosphorylation state with this perturbation, several proteins exhibited a dramatic change between control and high-Ca^{2+} conditions. Again, we focused on the proteins undergoing the largest change in phosphorylation state in this perturbation. These highly significant changes include PDH, MnSOD, and γF_1. It is important to note that these are the proteins exhibiting large alterations with Ca^{2+} and that more subtle changes in phosphorylation or effects on proteins at low concentrations were ignored in this initial screen. We did not detect a dephosphorylation of RISP in response to Ca^{2+} as suggested by isoelectric focusing shifts previously observed in liver mitochondria (*39*).

We focused on PDH and MnSOD for the remaining portion of this study since one, PDH, served as a control as

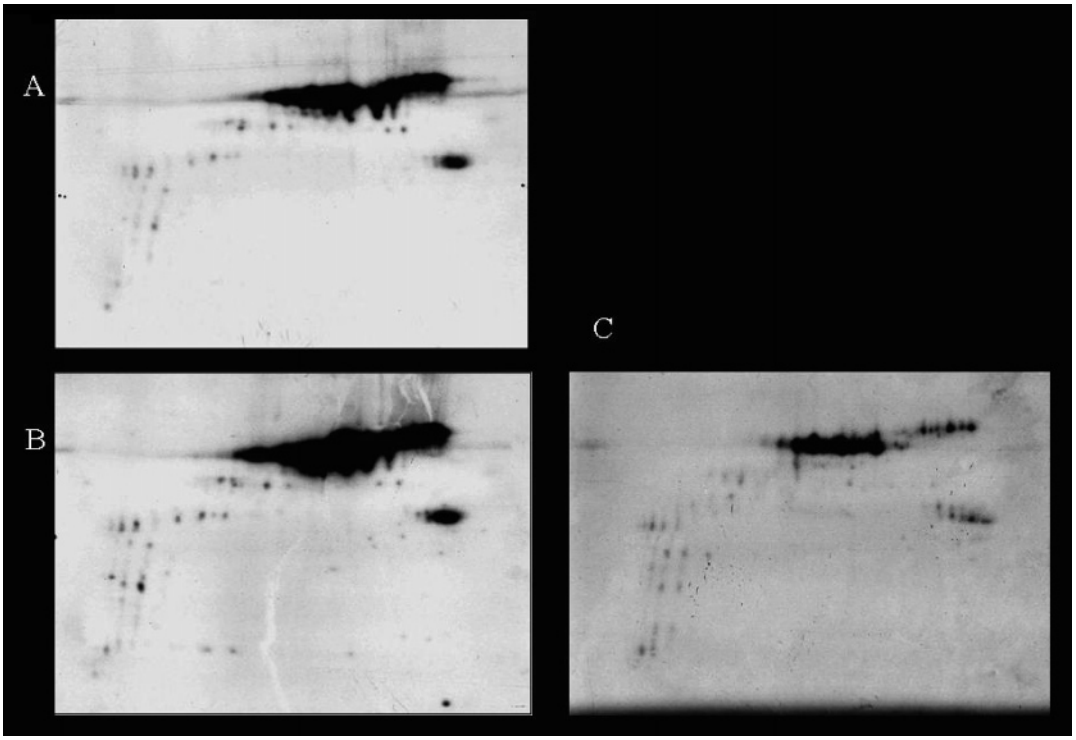

FIGURE 4: Two-dimensional gel electrophoresis and staining of the phosphoproteome of porcine heart mitochondria with [^{32}P]PO_4. Proteins are separated by isoelectric point (pI), from pH ~4 to 9 along the horizontal axis, and by molecular mass, from ~100 to 10 kDa, vertically. The mitochondria were harvested after incubation with [^{32}P]PO_4 for either 5 (A), 20 (B), or 20 min and then for 5 min with dinitrophenol, a mitochondrial uncoupler (C). The incubation conditions are outlined in Experimental Procedures.

a well-known protein phosphorylation affected by matrix Ca^{2+} while MnSOD is an important enzyme in ROS metabolism that was previously unknown as a phosphorylated protein in mammalian mitochondria.

Previous selective nonscreening studies demonstrated Ca^{2+}-induced dephosphorylation of the E1α subunit of PDH and activation of PDH (*12*, *40*). Consistent with these results, Pro-Q Diamond staining showed a dramatic dephosphorylation of the E1α subunit of PDH in the presence of Ca^{2+} (Figure 5A) that had the appropriate sensitivity to the extramitochondrial Ca^{2+} level. Four distinct PDH E1α subunit spots present in all Pro-Q Diamond-stained gels showed an average 63.1% decrease in the level of phosphorylation with Ca^{2+} ($n = 9$, $P < 0.05$; Figure 5B). The activity of PDH was increased by 203.6% ($n = 5$, $P < 0.05$) under the high-Ca^{2+} conditions that induced the dephosphorylation of the E1α subunit (Figure 5C). This confirmation of the well-known effects of Ca^{2+} on PDH phosphorylation provides a useful confirmation of this phosphoprotein screen.

Ca^{2+} exposure yielded an average 50.8% dephosphorylation of MnSOD ($n = 8$, $P < 0.05$; Figure 6A,B). To our knowledge, the phosphorylation of MnSOD has not previously been described in mammalian mitochondria. This enzyme is believed to play a critical role in the scavenging of ROS in the mitochondrial matrix. Thus, we further investigated the functional consequences of this dephosphorylation. The Ca^{2+} challenge resulted in an ~10-fold increase in the extent of mitochondrial H_2O_2 generation. Associated with this Ca^{2+}-induced increase in the level of H_2O_2 production was a 59.1% increase in MnSOD activity ($n = 3$, $P < 0.05$; Figure 6C). The extramitochondrial Ca^{2+} K_{50} of MnSOD activity was ~10 μM (Figure 6D). Since ROS production was stimulated by Ca^{2+}, we hypothesized that ROS could be directly responsible for the activation of MnSOD, independent of Ca^{2+}. This hypothesis was tested by generating similar levels of H_2O_2 production independent of Ca^{2+} and examining the effects on MnSOD phosphorylation and activity. The concentrations of rotenone and succinate were titrated to create a H_2O_2 generation rate (*41*) similar to that achieved under the high-Ca^{2+} conditions (Figure 7A). Unlike the high-Ca^{2+} conditions, the addition of rotenone and succinate did not induce significant release of cyt *c* (Figure 7B), indicating that a high level of ROS production alone is not sufficient to induce mitochondrial apoptosis, nor did it change MnSOD activity or phosphorylation state (Figure 7C,D). These data are consistent with a Ca^{2+}-dependent activation of MnSOD via dephosphorylation. In addition, the screen failed to detect any large changes in protein phosphorylation associated with the rotenone and succinate condition with the large increase in the level of H_2O_2 production, suggesting that acute ROS generation alone was not effective in modulating the phosphorylation state of PDH, γF_1, or other mitochondrial phosphoproteins that were detected (data not shown).

The dose dependence of Ca^{2+} on PDH and MnSOD phosphorylation was evaluated at four concentrations of free Ca^{2+} (0, 0.6, 40, and 100 μM) in paired experiments to determine whether these effects were due to the gross metabolic insult associated with Ca^{2+}-induced cyt *c* release. In addition, we could roughly compare the MnSOD phosphorylation level with activity to further establish cause and effect. The concentration of 0.6 μM was selected as the maximum Ca concentration for activating dehydrogenase and F1-ATPase activity in this preparation (*27*) without evidence of uncoupling or cyt *c* release. The concentration of 40 μM was selected as an intermediate value. The results of this

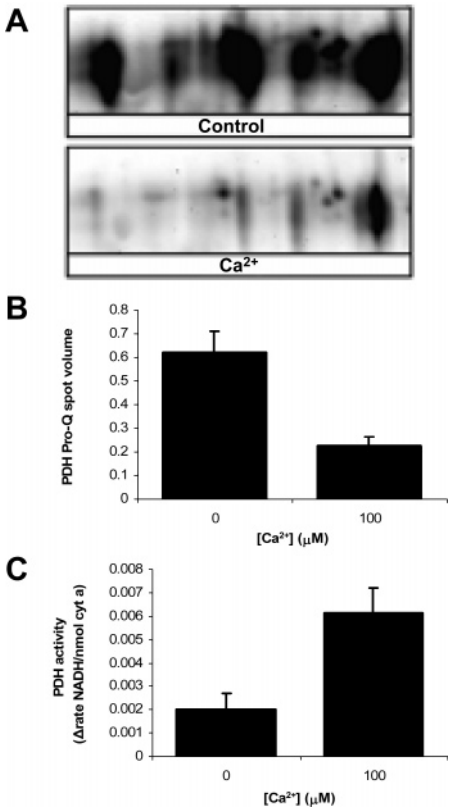

FIGURE 5: Effect of Ca^{2+} on PDH phosphorylation and activity. Representative images of gels stained with Pro-Q Diamond indicate the degree of PDH E1α phosphorylation of individual proteins with zero (top panel) or a high concentration of free Ca^{2+} (bottom panel) (A). Multiple protein spots of the pyruvate dehydrogenase E1α subunit stain with Pro-Q Diamond more intensely under control conditions than under high-Ca^{2+} conditions. The degree of phosphorylation under each condition was calculated as the ratio of intensity of Pro-Q staining for each spot to the total Sypro Ruby spot volume for that gel to normalize for any difference in total protein loaded in the gel and is given as the mean ± the standard error of the mean. (B) Because these proteins are highly phosphorylated but not abundant, matching spots from Pro-Q Diamond to Sypro Ruby images was difficult, and therefore, the total spot volume of the gel was used to normalize the amount of protein. The PDH enzyme activity increased in the presence of a high level of Ca^{2+} relative to control conditions (C).

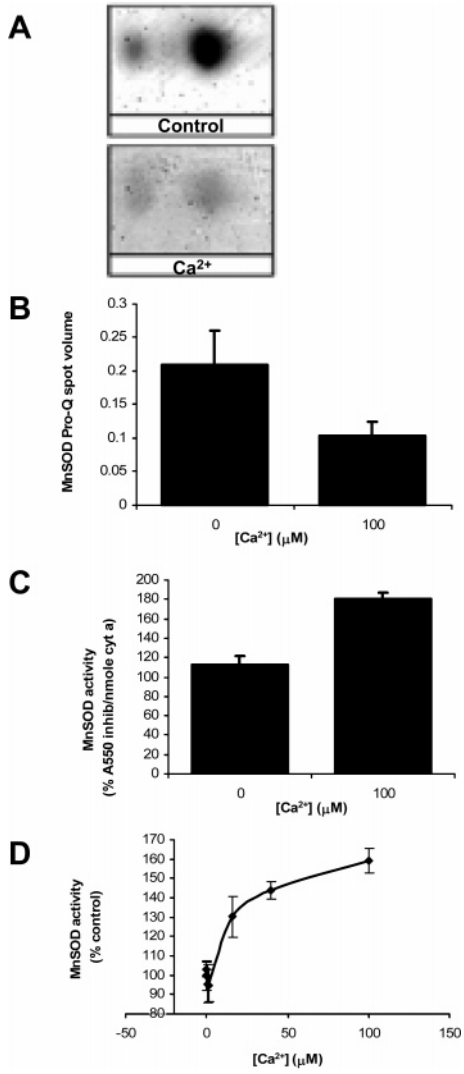

FIGURE 6: Effect of Ca^{2+} on MnSOD phosphorylation and activity. (A) MnSOD also exhibited less intense staining with Pro-Q Diamond under high-Ca^{2+} conditions (bottom panel) compared to control (top panel). The degree of phosphorylation under each condition was determined by the intensity of Pro-Q Diamond staining normalized to the corresponding Sypro Ruby intensity for that MnSOD spot (B). The activity of MnSOD normalized to cyt *a* content under control and high-Ca^{2+} conditions shows increased enzyme activity with the addition of Ca^{2+} (C). This increase is dependent on Ca^{2+} concentration. The dose−response curve of MnSOD activity over Ca^{2+} concentrations ranging from 0 to 100 μM free Ca^{2+}, expressed as the percent activity under control conditions, shows that the K_{50} is ~10 μM (D).

dosing study are presented in Figure 8. Both MnSOD and PDH had very similar responses to the addition of Ca^{2+} with the largest effect occurring with the addition of 0.6 μM Ca^{2+}, or the level activating ATP production under these Ca^{2+}-depleted conditions. This high Ca^{2+} affinity for dephosphorylation of MnSOD is consistent with the dose dependence of activity noted above (Figure 6D) with a K_{50} of ~10 μM. Clearly, a small Ca^{2+} dose that does not induce uncoupling or cyt *c* release resulted in a significant decrease in the level of phosphorylation. This result suggests that the dephosphorylation in these two proteins was not necessarily limited to the high levels of Ca used to mimic the apoptotic effects and potentially generate gross metabolic consequences.

The large number of phosphorylated enzymes detected in the mitochondrial matrix implies a very diverse and active system of kinases and phosphatases that might play a key role in the regulation of mitochondrial function, much like the scenario extensively described for PDH. To begin to unravel the mitochondrial kinase−phosphatase interactions, we conducted an initial screen for kinases, phosphatases, and sites of phosphorylation using a commercial antibody-based screening procedure. This screening procedure positively identified 11 kinases and three phosphatases (Table 2). Because of numerous confounding factors, such as dependence on antibody specificity, cross reactivity between mouse-specific antibodies and porcine proteins, and individual protein concentrations, this list cannot be considered comprehensive at this time. These results confirm previous studies localizing several of these kinases to mitochondria, including the MAP kinase system, Raf kinases, and lyn kinase (*21*, *22*). Most kinases localized to the mitochondria in this study have been associated with apoptosis signaling events, including p38 MAP kinase, stress-activated protein kinase (*42*), DNA-activated protein kinase (*43*), casein kinase II α (*44*), α IkBa α (*45*), ribosomal S6 protein kinase 1 (*46*),

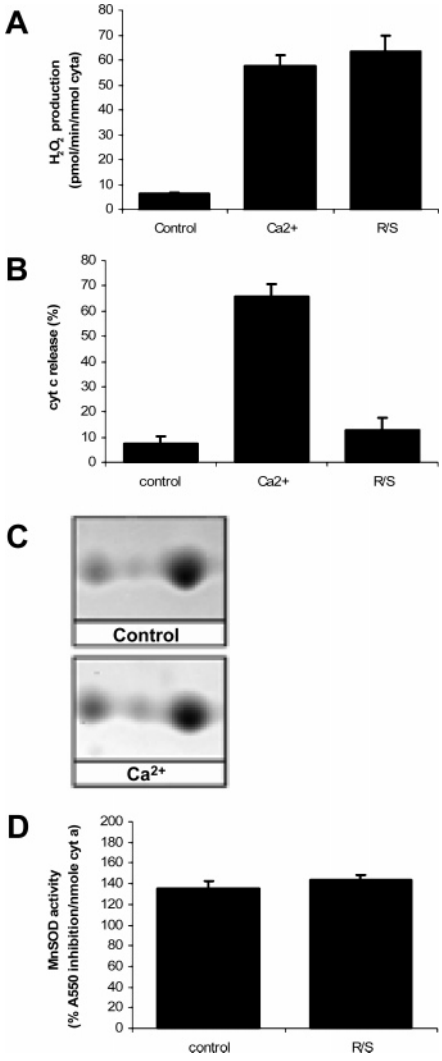

FIGURE 7: Effects of matrix ROS production on MnSOD phosphorylation and activity. The rate of H_2O_2 production per minute, normalized to cyt *a* content, shows that treatment of mitochondria with rotenone and succinate (R/S) increased the rate of H_2O_2 production significantly over control levels, similar to the increase induced by the high-Ca^{2+} conditions (A). Cyt *c* is released from mitochondria in the presence of a high concentration of Ca^{2+}, but not with R/S, indicating that the increased level of H_2O_2 production does not induce apoptosis (B). MnSOD spots in gels of mitochondria exposed to R/S show no change in Pro-Q Diamond staining intensity relative to control (C). MnSOD activity shows no significant difference under control and R/S conditions (D).

and protein kinase Cβ (*47*); however, how these might be linked to the phosphoproteome and effects of Ca^{2+} has yet to be resolved. The acute effects of extramitochondrial Ca^{2+} on the mitochondrial phosphoproteome resulted almost exclusively in dephosphorylation events; thus, phosphatases sensitive to Ca^{2+}, or conditions generated by Ca^{2+} addition, will be likely candidates for further investigation in this signaling process. Finally, though the mitochondrial preparation appears to be quite pure on the basis of the proteomic profiles obtained, we also cannot be certain that some of these postive results for kinases and phosphatases could be due to adhesion to the outside of the mitochondria and not present in the matrix, or caused by small contaminating structures from the cytosol. Confirmation of the localization of these enzymes within the matrix will be required.

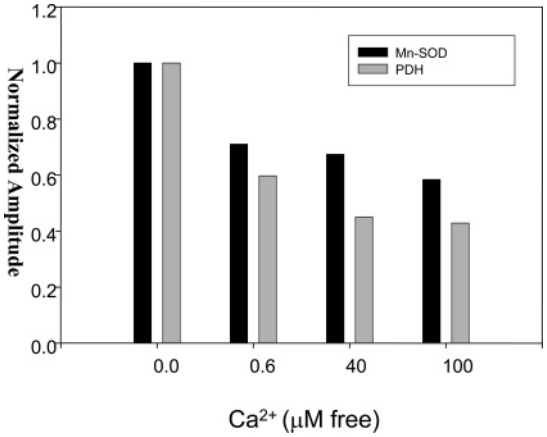

FIGURE 8: Ca^{2+} concentration dose dependence of PDH and MnSOD phosphorylation. Experiments were conducted under identical conditions as in Figures 5 and 6 with free Ca^{2+} concentrations of 0, 0.6, 40, and 100 μM.

Table 2: Antibody-Based Screen for Kinases and Phosphatases in Isolated Mitochondria

	protein name
kinases	
p38 hog CT	p38α MAP kinase (hog)
PKC-β1	protein kinase Cβ1
Mek1	MAP kinase kinase 1
DNAPK	DNA-activated protein kinase
Mek6	MAP kinase kinase 6
Rsk1 (C21)	ribosomal S6 kinase 1
CK2α-III	casein kinase 2α
IKKα (H744)	inhibitor NF-κB kinase α
Lyn (H-6)	oncogene Lyn
Raf1 (C20)	oncogene Raf 1
JAK1 (HR-785)	Janus kinase 1
phosphatases	
PP2A/A	protein phosphatase 2A, a regulatory subunit
PP2A/C	protein phosphatase 2A, a catalytic subunit
MKP-1 (V-15)	MAP kinase phosphatase 1
VHR	dual-specificity phosphatase 3

DISCUSSION

This study extends the knowledge of the mitochondrial phosphoproteome in the porcine heart using the Pro-Q Diamond staining procedure in conjunction with 2D gel electrophoresis−mass spectrometry approaches. Forty-five phosphorylated proteins were identified in total extracts of mitochondria, covering a wide range of functional attributes from membrane transport events to energy and ROS metabolism. Many of these phosophorylations are previously unknown, suggesting phosphorylation may be a more prominent regulatory mechanism in mitochondria than previously thought. The ^{32}P protein labeling in intact mitochondria confirmed the extensive nature of matrix protein phosphorylation as well as its dynamic nature required for an acute signaling network. In this study, we examined the interaction of Ca^{2+} and ROS, which are believed to activate complex metabolic and functional networks and are thought to play an important role in the regulation of energy metabolism as well as mitochondrion-initiated apoptosis.

The sensitivity of Pro-Q Diamond has been validated in several systems (*35*, *36*). The major advantage of Pro-Q Diamond that determines the total level of protein phosphorylation is that it functions in the steady state, not requiring phosphate turnover, as required for ^{32}P labeling experiments,

and can work in the presence of high concentrations of ATP without any concern of competition. However, many limitations exist for this type of screen. Gel-based techniques are inherently biased to detect the most abundant proteins and the most dramatic changes. Screening total protein phosphorylation limits detection if only few of many phosphorylation sites on one protein are affected by a signaling pathway. In addition, some have reported weak nonspecific protein staining with Pro-Q Diamond (*48*). ^{32}P labeling confirmed many of the Pro-Q phosphorylation sites, including PDH, MnSOD, inhibin, MCAD, LCAD, and Rieske iron−sulfur protein, but the patterns of ^{32}P and Pro-Q Diamond labeling were, not surprisingly, very different as discussed further below. Finally, the detection limits of Pro-Q Diamond for protein phosphorylation have not been extensively determined with regard to the number of phosphorylation sites required per protein. However, in some cases, we found that the Pro-Q Diamond stain was more sensitive for protein detection than Sypro Ruby staining (for example, PDH and cytochrome oxidase in Figure 2C), while several Pro-Q Diamond-stained proteins are yet to be determined due to sensitivity limits of mass spectroscopy. The latter results suggest that the sensitivity of Pro-Q Diamond for some protein phosphorylations is very good.

As discussed above, the ^{32}P labeling resulted in the detection of an extensive dynamic pool of phosphorylated proteins in the mitochondrial matrix. To our knowledge, this is the first demonstration of such extensive phosphorylation likely due to the nature of the protocol that generates predictably a nearly 100% ^{32}P specific activity for the γ-phosphate of ATP in the mitochondrial matrix. In these initial studies, we confirmed many of the proteins detected using Pro-Q Diamond but also detected many others that were in regions where Coomassie staining revealed no proteins, implying a high rate of phosphate turnover of a very small protein pool, ideal for acute signaling purposes. The initial time courses of labeling confirm a rapid phosphorylation turnover in the matrix (Figure 4). Adding uncoupler, which rapidly depletes the tiny matrix ATP pool, resulted in a dramatic decrease in the overall level of ^{32}P labeling and also confirmed that the protein phosphorylations were turning over at least on the minute time scale (compare panels B and C of Figure 4). This result also implies that the protein phosphorylation state could be sensitive to the matrix ATP levels, providing yet another potential feedback signal for energy metabolism.

The advantage of the ^{32}P labeling approach is that it is the gold standard with regard to the proof of association of a phosphate with a protein, but it also provides unique information about the turnover of the protein phosphorylation that is key in understanding signaling networks. One of the disadvantages is that care must be taken to avoid competition with cold phosphate, limiting the concentration of physiological substrates such as phosphate and ATP. This forces the ^{32}P labeling to be conducted under nonphysiological conditions and be very sensitive to the metabolic state of the mitochondria since exogenous ATP cannot be provided. Another complication with 32P ATP labeling is the possible tight interaction of ATP itself with a protein, rather than actual phosphorylation, that could lead to a false positive. The identity of many of the proteins seen in the ^{32}P screen will be difficult to unravel due to low abundance; however, these studies reveal a large network of protein phosphorylations that may play a key role in the acute and chronic regulation of mitochondrial function.

A dose of extramitochondrial Ca^{2+} was selected to induce cyt *c* release and simulate the initial stages of mitochondrion-induced apoptosis. This large dose of Ca^{2+} was used with the expectations that both the more sensitive energy metabolism activation processes and processes related to apoptosis and cyt *c* release could be captured in a single screen. We determined the optimal conditions for generating cyt *c* release for this preparation due to the wide variation in conditions found in the literature. We found a dependence of Ca^{2+}-induced cyt release on millimolar concentrations of both P_i and ATP. The mechanisms associated with the P_i and ATP requirements of Ca^{2+}-induced cyt *c* release remain poorly defined.

Extramitochondrial Ca^{2+} was found to dephosphorylate PDH, MnSOD, and γF_1. The dephosphorylation and activation of PDH serves as a useful control since the Ca^{2+} activation of pyruvate dehydrogenase phosphatase I, resulting in PDH dephosphorylation and activation, has been well established (*12*). The extensive phosphorylation of PDH observed with Pro-Q was confirmed in the ^{32}P labeling experiments as the most extensive phosphorylation site. In addition, the turnover of PDH phosphorylation was very fast based on the limited time course and rapid dephosphorylation with the uncoupler. The dose dependence of PDH dephosphorylation reaching a maximum at 600 nM was consistent with the metabolic actions of Ca, a stimulation previously established in this preparation, and not with the release of cyt *c* and general metabolic failure.

MnSOD, a matrix protein, converts superoxide to hydrogen peroxide and represents the primary mitochondrial defense against damage induced by superoxide radicals (*49*). Several lines of evidence support the notion that MnSOD is phosphorylated. (1) MnSOD was labeled with ^{32}P, confirming earlier work in potato mitochondria (*50*). (2) MnSOD was stained with Pro-Q Diamond. (3) Four protein spots with similar molecular masses but different isoelectric points were identified as MnSOD, consistent with protein phosphorylation. (4) The activity of MnSOD was inversely correlated with the extent of protein phosphorylation in the Ca^{2+} dose−response experiments (Figures 6D and 8). It is also interesting to note that the ^{32}P labeling was concentrated in the most acid-shifted form of MnSOD, consistent with the highest level of phosphorylation (see Figure 3). The ^{32}P labeling of MnSOD was not as extensive as that of other proteins, suggesting a relatively slow turnover of the phosphorylation site under steady-state conditions. The Ca^{2+}-sensitive dephosphorylation and activation of MnSOD is a novel finding and suggests that MnSOD activity may be controlled to regulate matrix levels of superoxide or hydrogen peroxide for other signaling processes. Potentially, the ROS generation stimulated by Ca^{2+} might be "buffered" by a parallel activation of the ROS scavenging MnSOD. Although the sites of phosphorylation of MnSOD remain to be determined, we speculate that the phosphorylation of Tyr34 may be a mechanism of inhibition of MnSOD activity. It was previously shown that reactive nitrogen species attack Tyr34 in the active site of MnSOD, causing nitration of the amino acid and subsequent inhibition of the enzyme (*51*, *52*). Phosphorylation of this tyrosine could protect the residue

from nitration but be made rapidly available by dephosphorylation when needed for enzyme activation. Attempts to dephosphorylate MnSOD with alkaline phosphatase protein phosphatase 1 were unsuccessful, suggesting that a specific phosphatase is likely responsible for the Ca^{2+} actions on the enzyme while the kinase also remains unknown at this time.

With the discovery of the effects of Ca^{2+} on MnSOD activity, we tested the hypothesis that matrix ROS generation alone could alter MnSOD phosphorylation and activity. Under the conditions of our study, we found weak effects of ROS generation on overall matrix protein phosphorylation. Specifically, we found no large effect of ROS generation on PDH and MnSOD phosphorylation or any other phosphorylated protein detected in the Pro-Q Diamond staining. We have not attempted these experiments on the turnover experiments with ^{32}P labeling. These data suggest that the secondary formation of ROS alone with Ca^{2+} is not responsible for the dephosphorylation of PDH or MnSOD under these experimental conditions. The site of ROS generation and the extent of ROS generation in this study was limited. Thus, other sites of ROS production or larger magnitudes of ROS production might yield different results.

In summary, we have shown that the phosphoproteome of the intact mitochondrial matrix is extensive and dynamic. Most of the major metabolic pathways within the matrix possess dynamic protein phosphorylation sites, while many of the sites observed have not yet been identified. These results are consistent with protein phosphorylation in the matrix playing a major role in acute cellular signaling for energy metabolism, as well as the numerous other functions of the mitochondrion.

REFERENCES

1. Gray, M. W. (1992) The endosymbiont hypothesis revisited, *Int. Rev. Cytol. 141*, 233−357.
2. Cavalier-Smith, T. (1987) The simultaneous symbiotic origin of mitochondria, chloroplasts, and microbodies, *Ann. N.Y. Acad. Sci. 503*, 55−71.
3. Westermann, B., and Neupert, W. (2003) 'Omics' of the mitochondrion, *Nat. Biotechnol. 21*, 239−240.
4. Richly, E., Chinnery, P. F., and Leister, D. (2003) Evolutionary diversification of mitochondrial proteomes: Implications for human disease, *Trends Genet. 19*, 356−362.
5. Taylor, S. W., Fahy, E., Zhang, B., Glenn, G. M., Warnock, D. E., Wiley, S., Murphy, A. N., Gaucher, S. P., Capaldi, R. A., Gibson, B. W., and Ghosh, S. S. (2003) Characterization of the human heart mitochondrial proteome, *Nat. Biotechnol. 21*, 281−286.
6. Mootha, V. K., Bunkenborg, J., Olsen, J. V., Hjerrild, M., Wisniewski, J. R., Stahl, E., Bolouri, M. S., Ray, H. N., Sihag, S., Kamal, M., Patterson, N., Lander, E. S., and Mann, M. (2003) Integrated analysis of protein composition, tissue diversity, and gene regulation in mouse mitochondria, *Cell 115*, 629−640.
7. Kernec, F., Unlu, M., Labeikovsky, W., Minden, J. S., and Koretsky, A. P. (2001) Changes in the mitochondrial proteome from mouse hearts deficient in creatine kinase, *Physiol. Genomics 6*, 117−128.
8. Liu, X. H., Qian, L. J., Gong, J. B., Shen, J., Zhang, X. M., and Qian, X. H. (2004) Proteomic analysis of mitochondrial proteins in cardiomyocytes from chronic stressed rat, *Proteomics 4*, 3167−3176.
9. Hunter, T. (2000) Signaling−2000 and beyond, *Cell 100*, 113−127.
10. Manning, G., Whyte, D. B., Martinez, R., Hunter, T., and Sudarsanam, S. (2002) The protein kinase complement of the human genome, *Science 298*, 1912−1934.
11. Cohen, P. (2002) The origins of protein phosphorylation, *Nat. Cell Biol. 4*, E127−E130.
12. Linn, T. C., Pettit, F. H., and Reed, L. J. (1969) α-Keto acid dehydrogenase complexes. X. Regulation of the activity of the pyruvate dehydrogenase complex from beef kidney mitochondria by phosphorylation and dephosphorylation, *Proc. Natl. Acad. Sci. U.S.A. 62*, 234−241.
13. Azarashvili, T. S., Tyynela, J., Odinokova, I. V., Grigorjev, P. A., Baumann, M., Evtodienko, Y. V., and Saris, N. E. (2002) Phosphorylation of a peptide related to subunit c of the F0F1-ATPase/ATP synthase and relationship to permeability transition pore opening in mitochondria, *J. Bioenerg. Biomembr. 34*, 279−284.
14. Papa, S., Sardanelli, A. M., Cocco, T., Speranza, F., Scacco, S. C., and Technikova-Dobrova, Z. (1996) The nuclear-encoded 18 kDa (IP) AQDQ subunit of bovine heart complex I is phosphorylated by the mitochondrial cAMP-dependent protein kinase, *FEBS Lett. 379*, 299−301.
15. Bender, E., and Kadenbach, B. (2000) The allosteric ATP-inhibition of cytochrome *c* oxidase activity is reversibly switched on by cAMP-dependent phosphorylation, *FEBS Lett. 466*, 130−134.
16. Chen, R., Fearnley, I. M., Peak-Chew, S. Y., and Walker, J. E. (2004) The phosphorylation of subunits of complex I from bovine heart mitochondria, *J. Biol. Chem. 279*, 26036−26045.
17. Hojlund, K., Wrzesinski, K., Larsen, P. M., Fey, S. J., Roepstorff, P., Handberg, A., Dela, F., Vinten, J., McCormack, J. G., Reynet, C., and Beck-Nielsen, H. (2003) Proteome analysis reveals phosphorylation of ATP synthase β-subunit in human skeletal muscle and proteins with potential roles in type 2 diabetes, *J. Biol. Chem. 278*, 10436−10442.
18. Schulenberg, B., Aggeler, R., Beechem, J. M., Capaldi, R. A., and Patton, W. F. (2003) Analysis of steady-state protein phosphorylation in mitochondria using a novel fluorescent phosphosensor dye, *J. Biol. Chem. 278*, 27251−27255.
19. Bykova, N. V., Egsgaard, H., and Moller, I. M. (2003) Identification of 14 new phosphoproteins involved in important plant mitochondrial processes, *FEBS Lett. 540*, 141−146.
20. Harris, R. A., Popov, K. M., Zhao, Y., Kedishvili, N. Y., Shimomura, Y., and Crabb, D. W. (1995) A new family of protein kinases: The mitochondrial protein kinases, *Adv. Enzyme Regul. 35*, 147−162.
21. Goldenthal, M. J., and Marin-Garcia, J. (2004) Mitochondrial signaling pathways: A receiver/integrator organelle, *Mol. Cell. Biochem. 262*, 1−16.
22. Thomson, M. (2002) Evidence of undiscovered cell regulatory mechanisms: Phosphoproteins and protein kinases in mitochondria, *Cell. Mol. Life Sci. 59*, 213−219.
23. Balaban, R. S. (2002) Cardiac energy metabolism homeostasis: Role of cytosolic calcium, *J. Mol. Cell. Cardiol. 34*, 1259−1271.
24. Dykens, J. A. (1994) Isolated cerebral and cerebellar mitochondria produce free radicals when exposed to elevated Ca^{2+} and Na^{+}: Implications for neurodegeneration, *J. Neurochem. 63*, 584−591.
25. Crompton, M. (1999) The mitochondrial permeability transition pore and its role in cell death, *Biochem. J. 341* (Part 2), 233−249.
26. Mattson, M. P., and Chan, S. L. (2003) Calcium orchestrates apoptosis, *Nat. Cell Biol. 5*, 1041−1043.
27. Territo, P. R., Mootha, V. K., French, S. A., and Balaban, R. S. (2000) Ca^{2+} activation of heart mitochondrial oxidative phosphorylation: Role of the F_0/F_1-ATPase, *Am. J. Physiol. 278*, C423−C435.
28. Lesnefsky, E. J., Moghaddas, S., Tandler, B., Kerner, J., and Hoppel, C. L. (2001) Mitochondrial dysfunction in cardiac disease: Ischemia−reperfusion, aging, and heart failure, *J. Mol. Cell. Cardiol. 33*, 1065−1089.
29. Palmer, J. W., Tandler, B., and Hoppel, C. L. (1985) Biochemical differences between subsarcolemmal and interfibrillar mitochondria from rat cardiac muscle: Effects of procedural manipulations, *Arch. Biochem. Biophys. 236*, 691−702.
30. Palmer, J. W., Tandler, B., and Hoppel, C. L. (1977) Biochemical properties of subsarcolemmal and interfibrillar mitochondria isolated from rat cardiac muscle, *J. Biol. Chem. 252*, 8731−8739.
31. Balaban, R. S., Mootha, V. K., and Arai, A. (1996) Spectroscopic determination of cytochrome *c* oxidase content in tissues containing myoglobin or hemoglobin, *Anal. Biochem. 237*, 274−278.
32. Wessel, D., and Flugge, U. I. (1984) A method for the quantitative recovery of protein in dilute solution in the presence of detergents and lipids, *Anal. Biochem. 138*, 141−143.
33. Neuhoff, V., Arold, N., Taube, D., and Ehrhardt, W. (1988) Improved staining of proteins in polyacrylamide gels including

isoelectric focusing gels with clear background at nanogram sensitivity using Coomassie Brilliant Blue G-250 and R-250, *Electrophoresis 9*, 255−262.
34. Robertson, J. G., Barron, L. L., and Olson, M. S. (1986) Effects of α-ketoisovalerate on bovine heart pyruvate dehydrogenase complex and pyruvate dehydrogenase kinase, *J. Biol. Chem. 261*, 76−81.
35. Schulenberg, B., Goodman, T. N., Aggeler, R., Capaldi, R. A., and Patton, W. F. (2004) Characterization of dynamic and steady-state protein phosphorylation using a fluorescent phosphoprotein gel stain and mass spectrometry, *Electrophoresis 25*, 2526−2532.
36. Chou, C. L., Christensen, B. M., Frische, S., Vorum, H., Desai, R. A., Hoffert, J. D., de Lanerolle, P., Nielsen, S., and Knepper, M. A. (2004) Non-muscle myosin II and myosin light chain kinase are downstream targets for vasopressin signaling in the renal collecting duct, *J. Biol. Chem. 279*, 49026−49035.
37. Unwin, R. D., Sternberg, D. W., Lu, Y., Pierce, A., Gilliland, D. G., and Whetton, A. D. (2005) Global effects of BCR/ABL and TEL/PDGFRβ expression on the proteome and phosphoproteome: Identification of the Rho pathway as a target of BCR/ABL, *J. Biol. Chem. 280*, 6316−6326.
38. Gunter, T. E., Yule, D. I., Gunter, K. K., Eliseev, R. A., and Salter, J. D. (2004) Calcium and mitochondria, *FEBS Lett. 567*, 96−102.
39. He, L., and Lemasters, J. J. (2005) Dephosphorylation of the Rieske iron−sulfur protein after induction of the mitochondrial permeability transition, *Biochem. Biophys. Res. Commun. 334*, 829−837.
40. Pettit, F. H., Roche, T. E., and Reed, L. J. (1972) Function of calcium ions in pyruvate dehydrogenase phosphatase activity, *Biochem. Biophys. Res. Commun. 49*, 563−571.
41. Turrens, J. F., and Boveris, A. (1980) Generation of superoxide anion by the NADH dehydrogenase of bovine heart mitochondria, *Biochem. J. 191*, 421−427.
42. Xia, Z., Dickens, M., Raingeaud, J., Davis, R. J., and Greenberg, M. E. (1995) Opposing effects of ERK and JNK-p38 MAP kinases on apoptosis, *Science 270*, 1326−1331.
43. Wang, S., Guo, M., Ouyang, H., Li, X., Cordon-Cardo, C., Kurimasa, A., Chen, D. J., Fuks, Z., Ling, C. C., and Li, G. C. (2000) The catalytic subunit of DNA-dependent protein kinase selectively regulates p53-dependent apoptosis but not cell-cycle arrest, *Proc. Natl. Acad. Sci. U.S.A. 97*, 1584−1588.
44. Guo, C., Yu, S., Davis, A. T., Wang, H., Green, J. E., and Ahmed, K. (2001) A potential role of nuclear matrix-associated protein kinase CK2 in protection against drug-induced apoptosis in cancer cells, *J. Biol. Chem. 276*, 5992−5999.
45. Fujihara, S., Jaffray, E., Farrow, S. N., Rossi, A. G., Haslett, C., and Hay, R. T. (2005) Inhibition of NF-κB by a cell permeable form of Iκ-Bα induces apoptosis in eosinophils, *Biochem. Biophys. Res. Commun. 326*, 632−637.
46. Harada, H., Andersen, J. S., Mann, M., Terada, N., and Korsmeyer, S. J. (2001) p70S6 kinase signals cell survival as well as growth, inactivating the pro-apoptotic molecule BAD, *Proc. Natl. Acad. Sci. U.S.A. 98*, 9666−9670.
47. Cao, M. Y., Shinjo, F., Heinrichs, S., Soh, J. W., Jongstra-Bilen, J., and Jongstra, J. (2001) Inhibition of anti-IgM-induced translocation of protein kinase CβI inhibits ERK2 activation and increases apoptosis, *J. Biol. Chem. 276*, 24506−24510.
48. Murray, J., Marusich, M. F., Capaldi, R. A., and Aggeler, R. (2004) Focused proteomics: Monoclonal antibody-based isolation of the oxidative phosphorylation machinery and detection of phosphoproteins using a fluorescent phosphoprotein gel stain, *Electrophoresis 25*, 2520−2525.
49. Fridovich, I. (1995) Superoxide radical and superoxide dismutases, *Annu. Rev. Biochem. 64*, 97−112.
50. Bykova, N. V., Stensballe, A., Egsgaard, H., Jensen, O. N., and Moller, I. M. (2003) Phosphorylation of formate dehydrogenase in potato tuber mitochondria, *J. Biol. Chem. 278*, 26021−26030.
51. MacMillan-Crow, L. A., Crow, J. P., and Thompson, J. A. (1998) Peroxynitrite-mediated inactivation of manganese superoxide dismutase involves nitration and oxidation of critical tyrosine residues, *Biochemistry 37*, 1613−1622.
52. Yamakura, F., Taka, H., Fujimura, T., and Murayama, K. (1998) Inactivation of human manganese-superoxide dismutase by peroxynitrite is caused by exclusive nitration of tyrosine 34 to 3-nitrotyrosine, *J. Biol. Chem. 273*, 14085−14089.

BI052475E